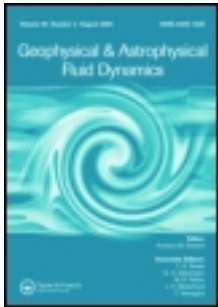


This article was downloaded by: [University of Helsinki], [Petri Käpylä]

On: 30 August 2012, At: 03:11

Publisher: Taylor & Francis

Informa Ltd Registered in England and Wales Registered Number: 1072954 Registered office: Mortimer House, 37-41 Mortimer Street, London W1T 3JH, UK



Geophysical & Astrophysical Fluid Dynamics

Publication details, including instructions for authors and subscription information:

<http://www.tandfonline.com/loi/ggaf20>

Oscillatory large-scale dynamos from Cartesian convection simulations

P.J. Käpylä^{a b c}, M.J. Mantere^a & A. Brandenburg^{b c}

^a Physics Department, University of Helsinki, Helsinki, Finland

^b NORDITA, Royal Institute of Technology and Stockholm University, Roslagstullsbacken 23, SE-10691 Stockholm, Sweden

^c Department of Astronomy, Stockholm University, SE-10691 Stockholm, Sweden

Version of record first published: 30 Aug 2012

To cite this article: P.J. Käpylä, M.J. Mantere & A. Brandenburg (2012): Oscillatory large-scale dynamos from Cartesian convection simulations, *Geophysical & Astrophysical Fluid Dynamics*, DOI:10.1080/03091929.2012.715158

To link to this article: <http://dx.doi.org/10.1080/03091929.2012.715158>



PLEASE SCROLL DOWN FOR ARTICLE

Full terms and conditions of use: <http://www.tandfonline.com/page/terms-and-conditions>

This article may be used for research, teaching, and private study purposes. Any substantial or systematic reproduction, redistribution, reselling, loan, sub-licensing, systematic supply, or distribution in any form to anyone is expressly forbidden.

The publisher does not give any warranty express or implied or make any representation that the contents will be complete or accurate or up to date. The accuracy of any instructions, formulae, and drug doses should be independently verified with primary sources. The publisher shall not be liable for any loss, actions, claims, proceedings, demand, or costs or damages whatsoever or howsoever caused arising directly or indirectly in connection with or arising out of the use of this material.

Oscillatory large-scale dynamos from Cartesian convection simulations

P.J. KÄPYLÄ†‡§*, M.J. MANTERE† and A. BRANDENBURG‡§

†Physics Department, University of Helsinki, Helsinki, Finland

‡NORDITA, Royal Institute of Technology and Stockholm University,
Roslagstullsbacken 23, SE-10691 Stockholm, Sweden

§Department of Astronomy, Stockholm University, SE-10691 Stockholm, Sweden

(Received 29 November 2011; in final form 20 July 2012)

We present results from compressible Cartesian convection simulations with and without imposed shear. In the former case the dynamo is expected to be of $\alpha^2\Omega$ type, which is generally expected to be relevant for the Sun, whereas the latter case refers to α^2 dynamos that are more likely to occur in more rapidly rotating stars whose differential rotation is small. We perform a parameter study where the shear flow and the rotational influence are varied to probe the relative importance of both types of dynamos. Oscillatory solutions are preferred both in the kinematic and saturated regimes when the negative ratio of shear to rotation rates, $q \equiv -S/\Omega$, is between 1.5 and 2, i.e. when shear and rotation are of comparable strengths. Other regions of oscillatory solutions are found with small values of q , i.e. when shear is weak in comparison to rotation, and in the regime of large negative qs , when shear is very strong in comparison to rotation. However, exceptions to these rules also appear so that for a given ratio of shear to rotation, solutions are non-oscillatory for small and large shear, but oscillatory in the intermediate range. Changing the boundary conditions from vertical field to perfect conductor ones changes the dynamo mode from oscillatory to quasi-steady. Furthermore, in many cases an oscillatory solution exists only in the kinematic regime whereas in the nonlinear stage the mean fields are stationary. However, the cases with rotation and no shear are always oscillatory in the parameter range studied here and the dynamo mode does not depend on the magnetic boundary conditions. The strengths of total and large-scale components of the magnetic field in the saturated state, however, are sensitive to the chosen boundary conditions.

Keywords: Solar dynamo; Convection; Turbulence

1. Introduction

The solar magnetic cycle is commonly thought to be a manifestation of an oscillatory large-scale dynamo operating within or just below the convection zone (e.g. Ossendrijver 2003). A possible origin of the solar magnetic fields is the turbulent dynamo mechanism, where helical small-scale fluid motions and large-scale shear sustain the magnetic field (e.g. Moffatt 1978, Krause and Rädler 1980,

*Corresponding author. Email: petri.kapyla@helsinki.fi

Rüdiger and Hollerbach 2004). According to mean-field theory, turbulent stratified convection together with global rotation of the Sun lead to an α effect (Steenbeck *et al.* 1966) and large-scale differential rotation (e.g. Rüdiger 1989). Their combined effect constitutes the $\alpha\Omega$ -dynamo, which often yields oscillatory solutions (e.g. Parker 1955, Steenbeck and Krause 1969).

However, reproducing the solar cycle with direct numerical simulations still remains challenging (e.g. Miesch and Toomre 2009, Käpylä 2011). Early spherical simulations were indeed able to achieve oscillatory large-scale fields that propagate toward the poles (Gilman 1983, Glatzmaier 1985). Similar results have been confirmed by a number of recent simulations in spherical shells (Brown *et al.* 2010, 2011a, Ghizaru *et al.* 2010, Racine *et al.* 2011) as well as in wedges of spherical shells (Käpylä *et al.* 2010d). Recent simulations in wedges have also yielded equatorward migration (Käpylä *et al.* 2012). Simpler Cartesian models with rotating stratified convection were less successful as only small-scale fields were seen (Nordlund *et al.* 1992, Brandenburg *et al.* 1996). Only when a shear flow was added (Käpylä *et al.* 2008, Hughes and Proctor 2009) or rapid enough rotation was used (Jones and Roberts 2000, Rotvig and Jones 2002, Käpylä *et al.* 2009b), large-scale fields were obtained. Even in the cases with imposed shear, no oscillatory solutions were seen although the necessary prerequisites, helical turbulence and shear were present. However, these are the aspects that depend critically on the boundary conditions. Indeed, (Käpylä *et al.* 2009c) have presented mean-field calculations of the associated convection simulations that agree with each other not only qualitatively in that both are non-oscillatory, but they also agree quantitatively as far as their excitation condition is concerned.

Here we extend previous studies on large-scale dynamos due to turbulent convection in Cartesian geometry (Käpylä *et al.* 2008, 2009b) to cover a larger parameter space and explore more thoroughly the effects of boundary conditions on the solutions. We present runs with imposed shear and find that oscillatory solutions can be found in a limited part of the parameter range studied. We also report on rigidly rotating runs where oscillatory α^2 -dynamos are observed.

2. Model

Our model setup is the same as that of Käpylä *et al.* (2008, 2009b). A rectangular portion of a star is represented by a box situated at colatitude θ . The dimensions of the computational domain are $(L_x, L_y, L_z) = (4, 4, 2)d$, where d is the depth of the convectively unstable layer, which is also used as the unit of length. The box is divided into three layers: an upper cooling layer, a convectively unstable layer, and a stable overshoot layer (see below). The following equations for compressible magnetohydrodynamics are solved:

$$\frac{\mathcal{D}A}{\mathcal{D}t} = -SA_y \hat{x} - (\nabla U)^T A - \eta \mu_0 \mathbf{J}, \quad (1)$$

$$\frac{\mathcal{D} \ln \rho}{\mathcal{D}t} = -\nabla \cdot \mathbf{U}, \quad (2)$$

$$\frac{\mathcal{D}\mathbf{U}}{\mathcal{D}t} = -S\mathbf{U}_x\hat{\mathbf{y}} - \frac{1}{\rho}\nabla p + \mathbf{g} - 2\boldsymbol{\Omega}_0 \times \mathbf{U} + \frac{1}{\rho}\mathbf{J} \times \mathbf{B} + \frac{1}{\rho}\nabla \cdot 2\nu\rho\mathbf{S}, \quad (3)$$

$$\frac{\mathcal{D}e}{\mathcal{D}t} = -\frac{p}{\rho}\nabla \cdot \mathbf{U} + \frac{1}{\rho}\nabla \cdot K\nabla T + 2\nu\mathbf{S}^2 + \frac{\mu_0\eta}{\rho}\mathbf{J}^2 - \frac{e - e_0}{\tau(z)}, \quad (4)$$

where $\mathcal{D}/\mathcal{D}t = \partial/\partial t + (\mathbf{U} + \overline{\mathbf{U}}_0) \cdot \nabla$ is the advective derivative with respect to the total (turbulent plus shear) flow, $\overline{\mathbf{U}}_0 = (0, Sx, 0)$ is the imposed large-scale shear flow, \mathbf{A} is the magnetic vector potential, $\mathbf{B} = \nabla \times \mathbf{A}$ is the magnetic field, $\mathbf{J} = \nabla \times \mathbf{B}/\mu_0$ is the current density, μ_0 is the magnetic permeability, η and ν are the magnetic diffusivity and kinematic viscosity, respectively, K is the heat conductivity, ρ is the density, \mathbf{U} is the velocity, $\mathbf{g} = -g\hat{\mathbf{z}}$ is the gravitational acceleration, and $\boldsymbol{\Omega}_0 = \Omega_0(-\sin\theta, 0, \cos\theta)$ is the rotation vector. The fluid obeys an ideal gas law $p = \rho e(\gamma - 1)$, where p and e are the pressure and internal energy, respectively, and $\gamma = c_p/c_v = 5/3$ is the ratio of specific heats at constant pressure and volume, respectively. The specific internal energy per unit mass is related to the temperature via $e = c_v T$. The traceless rate of strain tensor \mathbf{S} is given by

$$\mathbf{S}_{ij} = \frac{1}{2}(U_{ij} + U_{ji}) - \frac{1}{3}\delta_{ij}\nabla \cdot \mathbf{U}. \quad (5)$$

The last term of equation (4) describes cooling at the top of the domain. Here, $\tau(z)$ is a cooling time with a profile smoothly connecting the upper cooling layer and the convectively unstable layer below, where $\tau^{-1}(z) \rightarrow 0$. Let us note that equation (1) is here written in the fully advective gauge, but in practice, to avoid excessive buildup of gradient contributions to \mathbf{A} (Candelaresi *et al.* 2011), it is solved just in the shearing-advective gauge (see Hubbard and Brandenburg (2011) for details).

The positions of the bottom of the box, bottom and top of the convectively unstable layer, and the top of the box are given, respectively, by $(z_1, z_2, z_3, z_4) = (-0.85, 0, 1, 1.15)d$. Initially the stratification is piecewise polytropic with polytropic indices $(m_1, m_2, m_3) = (3, 1, 1)$, which leads to a convectively unstable layer above a stable layer at the bottom of the domain and an isothermal cooling layer at the top. All simulations with rotation use $\theta = 0$, corresponding to the north pole. Our initial stratification is given by the associated hydrostatic equilibrium solution (Brandenburg *et al.* 1996), where velocity and magnetic fields are perturbed with the Gaussian noise of low amplitude.

2.1. Nondimensional quantities and parameters

Dimensionless quantities are obtained by setting

$$d = g = \rho_0 = c_p = \mu_0 = 1, \quad (6)$$

where ρ_0 is the initial density at z_2 . The units of length, time, velocity, density, entropy, and magnetic field are

$$[x] = d, \quad [t] = \sqrt{d/g}, \quad [U] = \sqrt{dg}, \quad [\rho] = \rho_0, \quad [s] = c_p, \quad [B] = \sqrt{dg\rho_0\mu_0}. \quad (7)$$

The equipartition magnetic field is defined by

$$B_{\text{eq}} \equiv \langle \mu_0 \rho \mathbf{U}^2 \rangle^{1/2}, \quad (8)$$

where angle brackets denote volume averaging. We define the fluid and magnetic Prandtl numbers and the Rayleigh number as

$$\text{Pr} = \frac{\nu}{\chi_0}, \quad \text{Pm} = \frac{\nu}{\eta}, \quad \text{Ra} = \frac{gd^4}{\nu\chi_0} \left(-\frac{1}{c_p} \frac{ds}{dz} \right)_0, \quad (9)$$

where $\chi_0 = K/(\rho_m c_p)$ is the thermal diffusivity and ρ_m is the density in the middle of the convectively unstable layer, $z_m = z_3 - z_2$. The entropy gradient, measured at z_m in the non-convecting hydrostatic state, is given by

$$\left(-\frac{1}{c_p} \frac{ds}{dz} \right)_0 = \frac{\nabla - \nabla_{\text{ad}}}{H_P}, \quad (10)$$

where $\nabla - \nabla_{\text{ad}}$ is the superadiabatic temperature gradient with $\nabla_{\text{ad}} = 1 - 1/\gamma$, $\nabla = (\partial \ln T / \partial \ln p)_{z_m}$, where H_P is the pressure scale height. The degree of stratification is determined by the parameter $\xi_0 = (\gamma - 1)e_0/gd$, which is the pressure scale height at the top of the domain normalized by the depth of the unstable layer. We use $\xi_0 = 0.3$ in all cases, which results in a density contrast of about 23. We define the fluid and magnetic Reynolds numbers via

$$\text{Re} = \frac{u_{\text{rms}}}{\nu k_f}, \quad \text{Rm} = \frac{u_{\text{rms}}}{\eta k_f}, \quad (11)$$

where $k_f = 2\pi/d$ is assumed as a reasonable estimate for the wavenumber of the energy-carrying eddies. Note that, according to this definition, Rm is smaller than the usually adopted one by a factor 2π based on d instead of k_f . The amounts of shear and rotation are quantified by

$$\text{Sh} = \frac{S}{u_{\text{rms}} k_f}, \quad \text{Co} = \frac{2\Omega_0}{u_{\text{rms}} k_f}. \quad (12)$$

The denominators in equation (12) give an estimate of the inverse convective turnover time. We also use the value of the relative shear rate

$$q = -S/\Omega_0 = -2 \frac{\text{Sh}}{\text{Co}}, \quad (13)$$

which is often used in the context of disk systems, for which the local angular velocity varies like $\Omega(r) \propto r^{-q}$ with $q = 1.5$. For $q \geq 2$ the flow is Rayleigh unstable. Note that for $q = 2$, we have $2\Omega_0 + S = 0$, so the effect of rotation and shear, $SU_x \hat{y} + 2\Omega \times \mathbf{U} = (-2\Omega_0 U_y, (2\Omega_0 + S)U_x, 0)$, reduces to $(\tilde{S}U_y, 0, 0)$. Here we have introduced the quantity $\tilde{S} = -2\Omega_0$ to highlight the similarity to plane shear flow ($\Omega_0 = 0$), in which the effect of shear is given by $(0, SU_x, 0)$. This analogy between plane shear flow and marginally Rayleigh-stable flows was noted by Balbus *et al.* (1996) and will also play a role in our considerations below.

2.2. Boundary conditions

Stress-free boundary conditions are used for the velocity,

$$U_{x,z} = U_{y,z} = U_z = 0, \quad (14)$$

and either vertical field or perfect conductor conditions for the magnetic field, i.e.

$$B_x = B_y = 0 \quad (\text{vertical field}), \quad (15)$$

$$B_{x,z} = B_{y,z} = B_z = 0 \quad (\text{perfect conductor}), \quad (16)$$

respectively. We may think of them as open and closed boundaries, respectively, because they either do or do not permit a magnetic helicity flux. In the y and x directions we use periodic and shearing-periodic boundary conditions, respectively. In the runs with shear and rotation we use vertical field conditions at the top and perfect conductor conditions at the bottom, unless stated otherwise. The simulations have been made with the PENCIL CODE (<http://pencil-code.googlecode.com/>) using sixth-order explicit finite differences in space and a third-order accurate time stepping method.

3. Results

We perform three sets of simulations with our standard setup with shear and rotation (Sets A, B, and C) and a few exploratory runs with only rotation (Set D) (table 1). In the less extensive Sets E and F (table 2) we explore the parameter regime in the vicinity of one of the oscillatory models Run A2 (Set E), and the effect of changing boundary conditions on the solution (Set F). In Sets A and B we keep the shear rate S constant and vary the rotation rate Ω_0 . In Set A we use $S = -0.05\sqrt{g/d}$ and in Set B we have $S = -0.1\sqrt{g/d}$. In Set C the rotation rate $\Omega_0 = 0.1\sqrt{g/d}$ is fixed and the shear rate S is varied. Our hydrodynamical progenitors of the runs in Set A were taken from Käpylä *et al.* (2010b) and those of the runs in Set B were obtained by doubling both S and Ω_0 . In terms of q , we explore the range $-10. \dots 1.99$. We take Runs A9 and A1 from Käpylä *et al.* (2011) as the hydrodynamical progenitors for our runs in Set D with only rotation.

The case $S \neq 0$ and $\Omega_0 = 0$ corresponds to $q \rightarrow \pm\infty$ and is a special case in which a “vorticity dynamo” (e.g. Elperin *et al.* 2003, Käpylä *et al.* 2009a) is excited for the values of shear chosen here. In this part of the parameter range we use data from Käpylä *et al.* (2008) with $\Omega_0 = 0$ and $S \neq 0$. Values of q near zero refer to runs with rapid and nearly rigid rotation, whereas large values of $|q|$ are associated with strong shear and slow rotation. For $q \geq 2$ the flow is Rayleigh unstable, and thus we limit our study to values $q \leq 1.99$. However, in Set C we find large-scale vorticity generation for $q = 1.99$, leading eventually to supersonic velocities and numerical instability. In view of the analogy between plane shear flow and marginally Rayleigh-stable flows (section 2.1), this large-scale vorticity generation might be related to the aforementioned vorticity dynamo. Therefore we reduce the highest value of q to 1.95 in Set C. In many runs with $q > 0$ the rms-velocity increases in the saturated regime, which is likely due to the magnetorotational instability. This is particularly relevant in cases where the shear is strong, i.e. runs in Sets B and C.

In the following, we discuss first the case with shear and study the behavior of solutions for a range of values of q . We refer to these solutions as $\alpha\Omega$ (or α -shear) dynamos. We study separately the case without shear and refer to such solutions as α^2 dynamos, which are generally also known as $\alpha^2\Omega$ dynamos. We focus here specifically on the case of oscillatory solutions.

Table 1. Summary of the runs.

Run	Ma_{kin}	Ma	Rm	q	Co	Sh	\tilde{B}_{rms}	\tilde{B}_x	\tilde{B}_y	Mode	Comment
A1	0.036	0.031	25	1.99	0.26	-0.25	1.50	0.07	1.38	osc/osc?	
A2	0.034	0.029	23	1.75	0.31	-0.27	1.50	0.08	1.27	osc/osc	
A3	0.032	0.028	22	1.50	0.38	-0.28	1.58	0.10	1.29	osc/osc	
A4	0.030	0.027	22	1.25	0.46	-0.29	1.41	0.10	1.12	sta/osc?	
A5	0.032	0.028	22	1.00	0.57	-0.28	2.65	0.22	2.46	sta/sta	
A6	0.029	0.029	23	0.75	0.73	-0.27	3.34	0.29	3.16	sta/sta	
A7	0.031	0.030	24	0.50	1.07	-0.27	3.92	0.37	3.73	sta/sta	
A8	0.028	0.029	23	0.25	2.17	-0.27	4.34	0.47	4.08	sta/sta	
A9	0.017	0.026	20	0.10	6.19	-0.31	5.70	0.61	5.33	osc/sta	
A10	0.010	0.023	18	0.05	13.7	-0.34	7.07	0.75	6.53	osc/sta	
A11	0.011	0.011	8	-0.05	-30.2	-0.75	-	-	-	osc/-	Not run to saturation
A12	0.017	0.016	13	-0.10	-9.87	-0.49	-	-	-	osc/-	Not run to saturation
A13	0.023	0.056	45	-0.25	-1.13	-0.14	2.21	0.36	1.81	osc?/sta	
A14	0.026	0.062	49	-0.50	-0.52	-0.13	2.10	0.22	1.85	sta/sta	
A15	0.028	0.027	21	-1.0	-0.59	-0.30	-	-	-	sta/-	No dynamo
A16	0.030	0.028	23	-2.5	-0.22	-0.28	-	-	-	osc/-	No dynamo
A17	0.032	0.030	24	-5.0	-0.11	-0.26	-	-	-	osc/-	No dynamo
A18	0.037	0.036	28	-10.0	-0.04	-0.22	-	-	-	osc/-	No dynamo
B1	0.044	0.090	72	1.99	0.18	-0.18	1.15	0.09	1.00	osc/sta	
B2	0.036	0.040	32	1.75	0.46	-0.40	2.70	0.13	2.54	osc/osc?	
B3	0.031	0.039	31	1.50	0.54	-0.40	3.18	0.18	2.99	sta/sta	
B4	0.030	0.040	31	1.25	0.64	-0.40	3.22	0.20	3.03	sta/sta	
B5	0.032	0.042	33	1.00	0.77	-0.38	2.94	0.20	2.74	sta/sta	
B6	0.027	0.034	27	0.75	1.25	-0.47	3.79	0.34	3.57	sta/sta	
B7	0.025	0.038	31	0.50	1.66	-0.42	3.63	0.29	3.38	sta/sta	
B8	0.019	0.036	29	0.25	3.50	-0.44	4.00	0.33	3.68	osc/sta	
B9	0.011	0.029	23	0.10	11.0	-0.55	4.51	0.41	4.00	sta/sta	
B10	-	-	-	0.05	-	-	-	-	-	-	No convection
B11	-	-	-	-0.05	-	-	-	-	-	-	No convection
B12	0.011	0.011	8	-0.10	-30.2	-1.51	-	-	-	osc/-	Marginal dynamo
B13	0.020	0.018	15	-0.25	-6.91	-0.86	-	-	-	osc?/-	Not run to saturation
B14	0.024	0.086	69	-0.50	-0.74	-0.18	1.35	0.19	1.01	osc?/sta	
B15	0.027	0.094	75	-1.0	-0.34	-0.17	1.16	0.10	0.95	osc?/sta	
B16	0.032	0.030	24	-2.5	-0.43	-0.54	-	-	-	osc/-	Marginal dynamo
B17	0.037	0.032	26	-5.0	-0.20	-0.50	1.44	0.06	1.20	osc/sta	
B18	0.042	0.035	28	-10.0	-0.09	-0.46	1.61	0.08	1.35	osc/sta	
C1	0.055	0.165	131	1.95	0.19	-0.19	1.06	0.10	0.70	sta/osc	
C2	0.034	0.060	58	1.75	0.53	-0.46	2.32	0.15	1.99	sta/sta	
C3	0.031	0.050	50	1.50	0.64	-0.48	2.63	0.17	2.36	sta/sta	
C4	0.029	0.042	33	1.25	0.76	-0.47	3.22	0.20	3.00	sta/sta	
C5	0.029	0.039	31	1.00	0.83	-0.41	3.48	0.23	3.28	sta/sta	
C6	0.029	0.034	27	0.75	0.94	-0.35	3.91	0.27	3.73	sta/sta	
C7	0.029	0.030	24	0.50	1.06	-0.27	4.14	0.36	3.97	sta/sta	
C8	0.028	0.024	19	0.25	1.34	-0.17	3.35	0.54	3.11	sta/sta	
C9	0.027	0.020	16	0.10	1.58	-0.08	2.18	0.61	1.85	sta/sta	
C10	0.026	-	21	0.05	1.20	-0.03	-	-	-	sta/-	Not run to saturation
C11	0.026	-	21	-0.05	1.21	0.03	-	-	-	sta/-	No dynamo
C12	0.027	-	21	-0.10	1.18	0.06	-	-	-	sta/-	No dynamo
C13	0.027	-	21	-0.25	1.18	0.15	-	-	-	sta/-	Not run to saturation
C14	0.027	-	22	-0.50	1.16	0.29	-	-	-	sta/-	Not run to saturation
C15	0.028	-	23	-1.0	1.12	0.56	-	-	-	sta/-	Not run to saturation
C16	0.033	-	27	-2.0	0.95	0.95	-	-	-	sta/-	Not run to saturation
C17	0.061	-	48	-5.0	0.52	1.31	-	-	-	osc/-	Marginal dynamo

(Continued)

Table 1. Continued.

Run	Ma_{kin}	Ma	Rm	q	Co	Sh	\tilde{B}_{rms}	\tilde{B}_x	\tilde{B}_y	Mode	Comment
D1	0.081	0.021	66	<i>0</i>	4.60	0	1.18	0.30	0.31	osc/osc	Pm = 2, pc/vf
D1b	—	0.025	39	<i>0</i>	3.85	0	0.36	0.09	0.09	osc/osc	Pm = 1, pc/vf
D1c	—	0.032	26	<i>0</i>	2.96	0	0	0	0	osc/—	
D1d	0.083	0.021	66	<i>0</i>	4.60	0	1.18	0.32	0.29	osc/osc	Pm = 2, vf/vf
D1e	0.083	0.023	72	<i>0</i>	4.22	0	0.54	0.10	0.09	osc/osc	Pm = 2, pc/pc
D2	0.057	0.018	58	<i>0</i>	17.5	0	0.64	0.10	0.10	osc/osc	Pm = 2, pc/vf

Note: Ma_{kin} and Ma are the volume-averaged rms-velocities from the kinematic and saturated states, respectively. In Sets A and B we use $Pr = 1$, $Ra = 10^6$, $Pm = 1$, and grid resolution 128^3 . Perfect conductor (vertical field) conditions for the magnetic field at the lower (upper) boundary are used. In Set D, Pm varies, while $Pr = 0.24$, $Ra = 2 \times 10^6$, $Sh = 0$, and grid resolution 256×128^2 . The boundary conditions in Set D are listed in the rightmost column of the table. Oscillatory (osc) and stationary (sta) modes of the dynamo are denoted in the second column from right. Oscillatory decay is marked by “osc/—” with the comment “no dynamo”. For both types of oscillatory solutions, the q values are indicated in italics. Question marks indicate that only very few sign changes are covered by the time series or irregular reversals are seen. Here, $\tilde{B}_{\text{rms}} = B_{\text{rms}}/B_{\text{eq}}$, where B_{rms} is the total rms magnetic field, and $\tilde{B}_i = \langle \tilde{B}_i^2 \rangle^{1/2}/B_{\text{eq}}$.

Table 2. Summary of the additional runs.

Run	Ma_{kin}	Ma	Rm	q	Co	Sh	\tilde{B}_{rms}	\tilde{B}_x	\tilde{B}_y	Mode	Comment
E1	0.031	0.022	18	1.75	0.14	−0.12	1.18	0.11	0.90	sta/sta	
E2	0.033	0.027	21	1.75	0.24	−0.21	1.30	0.08	1.06	osc/osc	
E3	0.034	0.029	23	1.75	0.31	−0.27	1.50	0.08	1.27	osc/osc	Same as Run A2
E4	0.037	0.031	25	1.75	0.41	−0.36	2.09	0.10	1.87	osc/osc	
E5	0.037	0.053	42	1.75	0.51	−0.45	2.72	0.15	2.47	sta/sta	
F1	0.034	0.029	23	1.75	0.31	−0.27	1.50	0.08	1.27	osc/osc	pc/vf, same as Run A2
F2	0.034	0.029	23	1.75	0.31	−0.27	0.82	0.06	1.33	osc/osc	vf/vf
F3	0.034	0.029	23	1.75	0.31	−0.27	1.51	0.10	1.33	sta/sta	pc/pc

3.1. $\alpha^2\Omega$ dynamos

In our previous studies of convection-driven large-scale dynamos with shear (Käpylä *et al.* 2008, 2009b, 2010a), only non-oscillatory solutions were obtained. The large-scale field often had opposite signs in the convectively unstable and stable layers, although solutions with a single sign were obtained at low-magnetic Reynolds numbers (see figure 5 of Käpylä *et al.* 2010a) and in cases where $\Omega_0 = 0$ (see figure 7 of Käpylä *et al.* 2008). Runs with sinusoidal shear and rotation have also been reported to show non-oscillatory large-scale fields (Hughes and Proctor 2009, Käpylä *et al.* 2010c). In this paper, we extend the parameter ranges of our previous studies in search of oscillatory solutions. In this section we describe the results from different sets of runs individually, and summarize the results for the different dynamo modes in section 3.1.5.

3.1.1. $S = \text{const}$, Ω_0 varies (Sets A and B). As is evident from table 1, many of the runs in Sets A and B are non-oscillatory (see figure 1(a) for a representative result from Run A6). For Set A the mean magnetic field shows reversals in the range $1.5 \lesssim q < 2$, while the increased Ω_0 in Set B pushes the oscillatory regime somewhat toward higher qs . The oscillations are particularly clear in the kinematic regime in Runs A1–A3. Cycles in the non-linear regime are more irregular and in one case the dynamo mode

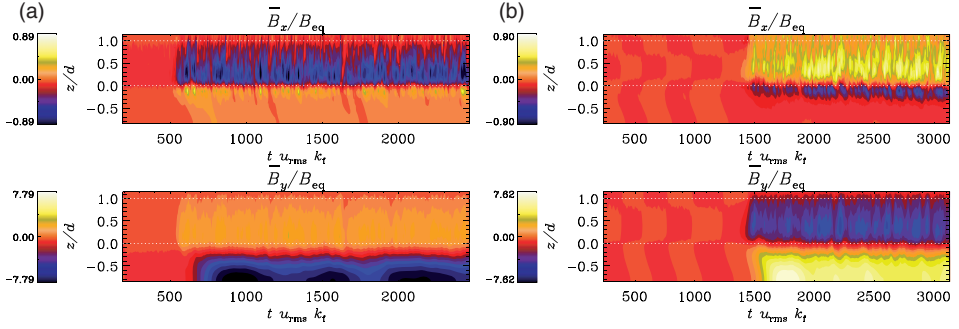


Figure 1. Horizontally averaged horizontal components of the magnetic field from non-oscillatory Run A6 (a) and initially oscillatory but ultimately stationary Run B8 (b) α -shear dynamos.

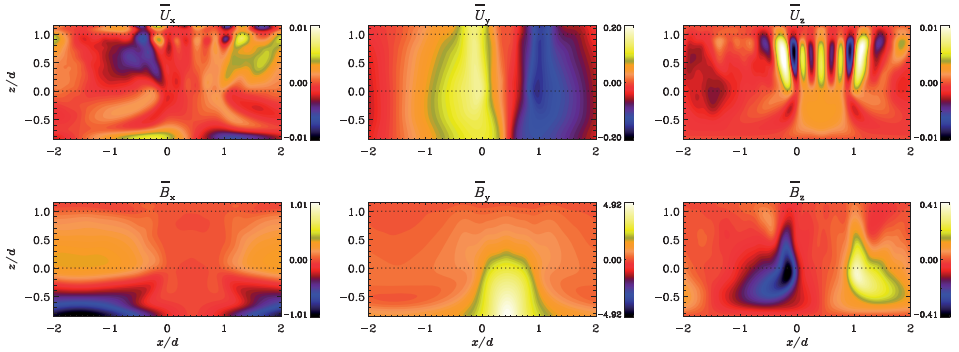


Figure 2. Mean velocities (upper row) and magnetic fields (lower row) averaged over the y -direction and time from Run B14. The velocities are shown in units of \sqrt{dg} and the magnetic fields in units of volume-averaged equipartition field B_{eq} .

changes to a non-oscillatory mode (Run B1). We find that in the parameter regime explored here, non-oscillatory solutions are excited in the range $0.2 \lesssim q < 1.5$. For $-10 \leq q \lesssim 0.25$, however, another oscillatory regime is found. These runs tend to show oscillations in the kinematic stage, but often switch to a stationary mode in the non-linear regime (see the time evolution of the horizontally averaged magnetic field components of Run B8 in figure 1(b)). This might just be a manifestation of the fact that the excitation conditions for different dynamo modes do not necessarily reflect the stable dynamo mode in the nonlinear regime (Brandenburg *et al.* 1989). This behavior also explains the lack of oscillatory dynamos in our previous works, where we always used $q = 1$. This further illustrates the importance of comprehensive parameter studies instead of individual numerical experiments (Käpylä *et al.* 2010b).

Convection is suppressed especially near $q = 0$ due to the rapid rotation, decreasing the Reynolds number and thus also leading to the absence of dynamo action in this regime. Many runs in the $q < 0$ regime, especially in Set A, are either subcritical or show very slow growth of the magnetic field and were not run to saturation. This lack of dynamo action may seem surprising because in the $q < 0$ regime the contributions to the α effect due to shear and rotation have the same sign (Käpylä *et al.* 2009b). On the

other hand, the magnetorotational instability can be excited for $q > 0$, which may explain the more favourable dynamo excitation in that regime. However, we find that if a saturated dynamo is present in this regime, also the turbulence is enhanced (see Runs A13, A14, B14, and B15). This is associated with the generation of additional large-scale flows that depend on x (figure 2). The large-scale magnetic fields are generally also x -dependent. Such modes are not visible in the kinematic stages of the runs.

3.1.2. S varies, $\Omega_0 = \text{const}$ (Set C). In Set C, only Run C17 with the strongest shear shows oscillations in the kinematic regime. The large-scale field in Run C1 shows oscillations in the nonlinear stage. We note that this is the only stable-to-oscillatory transition in the whole series of models explored. In the kinematic stage of this run, we observe an rms-velocity enhanced by almost a factor of two in comparison to Run C2. The only difference between these runs is a 10% smaller value of S for Run C2. The enhancement is likely to be due to the large-scale flows generated by the vorticity dynamo. Furthermore, as the magnetic field grows, the rms-velocity increases by another factor of three, which may be attributed to the magnetorotational instability. Similarly as in Sets A and B, the dynamo is harder to excite for $q < 0$ and in many cases the growth rate of the magnetic field is low, which is the reason why some of the runs were not continued up to saturation.

3.1.3. Sets E and F. It appears that small changes of Co and Sh are enough to change the dynamo mode, e.g. compare Runs B2 and C2 with $q = 1.75$. In Set E we vary Co and Sh , taking an oscillatory Run A2 as our basis (table 2). We find that oscillatory solutions are found in the intermediate range $0.24 < Co < 0.41$, corresponding to $0.21 < -Sh < 0.36$, whereas for lower and higher values of Co and Sh quasi-steady solutions appear.

In Set F we vary the magnetic boundary conditions of Run A2 and find that for perfect conductor boundaries at the top and bottom of the domain, the solution is non-oscillatory. For a vertical field condition on both boundaries, an oscillatory solution is found.

3.1.4. Cycle frequency and phase diagrams. Even in the cases with the clearest oscillatory solutions, e.g. Run A2 in figure 3(a), the period of the oscillation varies from cycle to cycle. Furthermore, the cycle period is of the order of 10^3 convective turnover times in this run. Such a long-cycle period limits the duration of the simulation to only a few cycles.

The cycle frequency of a saturated α -shear dynamo under the assumption of homogeneity is given by

$$\omega_{\text{cyc}} = \eta_{\text{T}} k_{\text{m}}^2, \quad (17)$$

where $\eta_{\text{T}} = \eta_{\text{t}} + \eta$ is the total magnetic diffusivity, η_{t} is the turbulent diffusivity, and k_{m} is the wavenumber of the dominant mode of the magnetic field (Blackman and Brandenburg 2002). Empirically, a similar law ($\omega_{\text{cyc}}/\eta_{\text{T}}k_{\text{m}}^2 = 1.6 \dots 2.3$) was also found for oscillatory α^2 dynamos with nonuniform helicity distribution (Brandenburg *et al.* 2008). Since equation (17) is also valid in the non-linear regime, the quenching of η_{t} as a function of Rm and \overline{B} can be estimated (Käpylä and Brandenburg 2009).

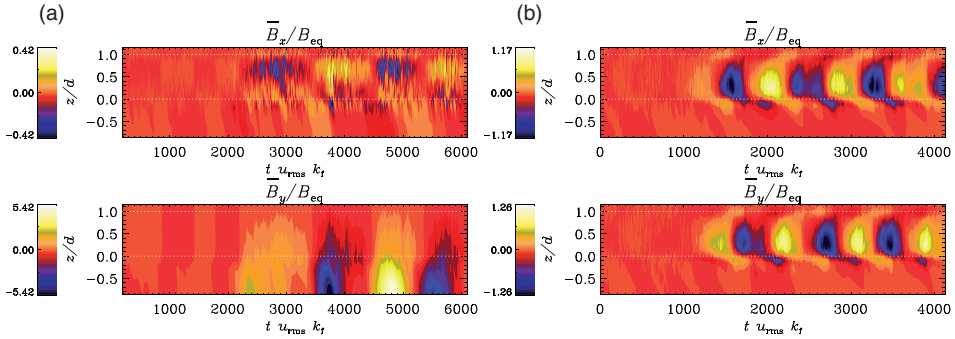


Figure 3. Same as figure 1 but for oscillatory α -shear dynamo Run A2 (a) and α^2 dynamo Run D1 (b).

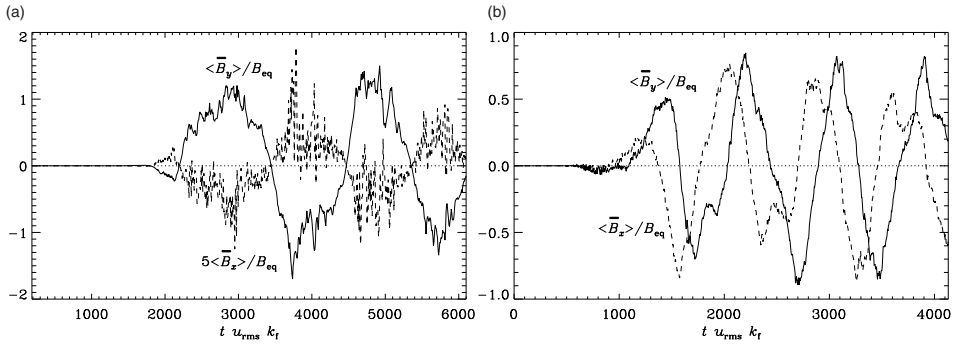


Figure 4. Phase diagrams for the same runs as in figure 3.

Although equation (17) is expected to be inaccurate in the present case, where the value of k_m is uncertain, the cycle frequency is likely regulated by the value of η_t . This suggests that the turbulent diffusivity is quenched by a factor of roughly two to three in Run A2, compared to the kinematic stage of the same run. This is entirely consistent with independent measurements of η_t , using the quasi-kinematic test-field method for quenched α^2 dynamos (Brandenburg *et al.* 2008).

The phase diagram of the horizontal components of the large-scale field averaged over $0.2d < z < 0.8d$ in Run A2 are shown in figure 4(a). The streamwise and cross-stream field components are in antiphase in this case. This is expected because S is negative (Stix 1976), so a positive B_x produces a negative B_y when $S < 0$.

3.1.5. Summary. The occurrence of oscillatory and quasi-steady solutions is conveniently discussed in parameter space where these types of solutions are marked in a Sh–Co diagram (see figure 5(a) and (b) for the kinematic and saturated regimes, respectively). Both coordinate axes are stretched by taking the square root, i.e. we use $\pm\sqrt{|\text{Sh}|}$, where upper and lower signs refer to the sign of Sh (and likewise for Co). Oscillatory solutions mainly occur in two branches near $q=2$ for $-\text{Sh} > 0.2$ and near $\text{Sh}=0$ for high enough Co (section 3.2). This is also true of the kinematic regime, but in

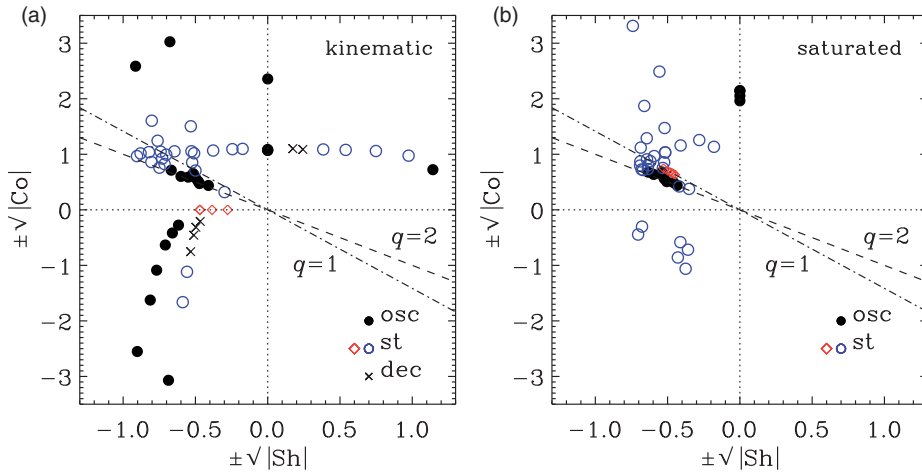


Figure 5. Dynamo mode in the kinematic regime (a) and in the saturated stage (b). Filled circles indicate oscillatory solutions and open circles (red and blue) quasi-steady ones. Red diamonds are data from Käpylä *et al.* (2008). Crosses indicate decaying solutions. Dashed and dash-dotted lines mark the positions of $q=1$ and 2, respectively.

that case there are additional occurrences of oscillatory solutions for strong negative shear and both signs of Co (figure 5(a)). Results from spherical geometry suggest that the appearance of cyclic magnetic fields depends also on the magnetic Reynolds number (Brown *et al.* 2011b).

3.2. Oscillatory α^2 dynamos

In an earlier study we found the appearance of large-scale magnetic fields in rigidly rotating convection (Käpylä *et al.* 2009b). However, none of the runs in that paper were run for much more than 10^3 convective turnover times. Although sign changes of the large-scale fields were seen (see figure 7 of Käpylä *et al.* 2009b), the time series were too short to enable any firm conclusions regarding the possibly oscillatory nature of the dynamo.

Furthermore, in similar rapidly rotating runs without magnetic fields, the appearance of large-scale vortices has been discovered (Chan 2007, Käpylä *et al.* 2011, Mantere *et al.* 2011). Here we use the hydrodynamical states of runs with large-scale cyclones as initial conditions for our dynamo simulations. We find that a large-scale dynamo is excited provided the magnetic Reynolds number exceeds a certain critical value. Furthermore, as the magnetic fields become dynamically important, the cyclones decay and are absent in the non-linear stage. The large-scale magnetic field is oscillatory in the two cases with different values of Co that we have considered. We conjecture that the dynamo is of α^2 type in which case oscillatory solutions can be excited if the α -effect has a suitable spatial profile (e.g. Baryshnikova and Shukurov 1987, Rüdiger *et al.* 2003, Mitra *et al.* 2010). Figure 3(b) shows the horizontally averaged mean magnetic fields from a rigidly rotating Run D1 where an α^2 dynamo is excited. In Run D1 the large-scale fields are only functions of z , whereas in the more rapidly rotating Run D2 the

large-scale fields depend also on x and y . Furthermore, the oscillatory nature of the solution is then not so clear. Figure 4(b) shows the phase diagram of the horizontal components of the large-scale field in Run D1. There is a phase shift of $\pi/2$.

The saturation level of the dynamo is sensitive to the magnetic Reynolds number. Decreasing Rm from 66 to 39 by doubling the value of η decreases the saturation field strength by a factor of three (Run D1b). Another doubling of η shuts the dynamo off (Run D1c).

Our standard setup in the present paper is to use perfect conductor boundaries at the bottom and vertical field conditions at the top. Changing the lower boundary also to vertical field conditions produces no discernible difference in the solution (Run D1d). However, imposing perfect conductor conditions on both boundaries decreases the saturation strength to less than a half of that in the standard setup and decreases the fraction of the large-scale field (Run D1e), but the solutions remain oscillatory. We have not, however, studied the Rm -dependence of the saturation field strength in this case, as was done in Käpylä *et al.* (2010a).

4. Conclusions

We have presented results from simulations of turbulent magnetized convection, both with an imposed shear flow using the shearing box approximation (Sets A, B, E, and F) and in rigidly rotating cases (Set D). In accordance with previous results, we find the generation of dynamically important large-scale magnetic fields. In distinction to our earlier studies, we vary here the relative importance of rotation and shear by covering the range $q = -10. \dots 1.99$ of the relative shear rate q . We find that for $q = 1$ the solutions are always stationary, which is in accordance with earlier results. In Sets A and B, where the shear is kept constant and the rotational influence is varied, oscillatory solutions are found for large q , i.e. slower rotation, and for $q \ll 1$. These trends are particularly clear in the kinematic regime. In the saturated state, however, we often find that the dynamo switches from oscillatory to stationary. In Set C, where $\Omega_0 = \text{const}$, only a single run shows oscillatory magnetic field in the saturated regime. Keeping q fixed and varying Co and Sh shows that oscillatory solutions appear only in the rather narrow range $0.24 < Co < 0.41$. Furthermore, when a perfect conductor boundary condition is adopted also at the top, the dynamo changes to a quasi-steady mode. Similar dependencies on boundary conditions can also be found in mean-field dynamos and are usually in agreement with corresponding DNS. These results suggest that a more thorough parameter study is needed and that the direct simulations need to be compared with mean-field models with the same parameters and turbulent transport coefficients from the test-field method. However, such a study is out of scope of the present paper.

It might not be easy to find general rules governing the transitions from oscillatory to non-oscillatory behavior in the parameter space defined by shear and rotation rates in the kinematic and nonlinear regimes. The simple rule that dynamos with shear oscillate while those without shear do not, is only safe in homogeneous systems without boundaries. For example, in the rigidly rotating cases of Set D, all the dynamo solutions are found to be oscillatory. In some cases, suitable spatial profiles of the resulting α effect have been found to be responsible for oscillatory behavior (e.g. Baryshnikova and

Shukurov 1987, Rüdiger *et al.* 2003, Mitra *et al.* 2010). Large-scale vortices, present in the hydrodynamic state, are no longer found in the saturated state of the dynamo. Usage of a perfect conductor boundary condition instead of a vertical field condition, allowing for magnetic helicity fluxes, is found to decrease both the total saturation field strength and the strength of the large-scale field with respect to the total magnetic field. This might be a consequence of what is known as catastrophic (or Rm-dependent) quenching, which cannot easily be alleviated in a closed domain, but it might also be a consequence of a delayed onset of dynamo action, which is explained by linear theory. In fact, recent work on catastrophic quenching has shown that resistive effects tend to dominate over effects resulting from magnetic helicity fluxes for magnetic Reynolds numbers below a value of around 10^3 or even 10^4 (Candelaresi *et al.* 2011). This makes an explicit demonstration of alleviated catastrophic quenching hard at the Rm values available to date.

Acknowledgements

We thank the three anonymous referees for making useful suggestions. The computations have been carried out using the facilities hosted by the CSC – IT Center for Science in Espoo, Finland, who are financed by the Finnish ministry of education. This work was supported in part by the European Research Council under the AstroDyn Research Project No. 227952, the Swedish Research Council Grant No. 621-2007-4064, and the Academy of Finland grants 136189, 140970 (PJK) and 218159, 141017 (MJM).

References

- Balbus, S.A., Hawley, J.F. and Stone, J.M., Nonlinear stability, hydrodynamical turbulence, and transport in disks. *Astrophys. J.* 1996, **467**, 76–86.
- Baryshnikova, I. and Shukurov, A., Oscillatory alpha-squared dynamo – numerical investigation. *Astron. Nachr.* 1987, **308**, 89–100.
- Blackman, E.G. and Brandenburg, A., Dynamic nonlinearity in large-scale dynamos with Shear. *Astrophys. J.* 2002, **579**, 359–373.
- Brandenburg, A., Candelaresi, S. and Chatterjee, P., Small-scale magnetic helicity losses from a mean-field dynamo. *Mon. Not. R. Astron. Soc.* 2009, **398**, 1414–1422.
- Brandenburg, A., Jennings, R.L., Nordlund, Å., Rieutord, M., Stein, R.F. and Tuominen, I., Magnetic structures in a dynamo simulation. *J. Fluid Mech.* 1996, **306**, 325–352.
- Brandenburg, A., Krause, F., Meinel, R., Moss, D. and Tuominen, I., The stability of nonlinear dynamos and the limited role of kinematic growth rates. *Astron. Astrophys.* 1989, **213**, 411–422.
- Brandenburg, A., Rädler, K.-H., Rheinhardt, M. and Subramanian, K., Magnetic quenching of alpha and diffusivity tensors in helical turbulence. *Astrophys. J.* 2008, **687**, L49–L52.
- Brown, B.P., Browning, M.K., Brun, A.S., Miesch, M.S. and Toomre, J., Persistent magnetic wreaths in a rapidly rotating Sun. *Astrophys. J.* 2010, **711**, 424–438.
- Brown, B.P., Miesch, M.S., Browning, M.K., Brun, A.S. and Toomre, J., Magnetic cycles in a convective dynamo simulation of a young solar-type star. *Astrophys. J.* 2011a, **731**, 69.
- Brown, B.P., Browning, M.K., Brun, A.S., Miesch, M.S. and Toomre, J., Global-scale wreath-building dynamos in stellar convection zones. *IAUS* 2011b, **271**, 78–85.
- Candelaresi, S., Hubbard, A., Brandenburg, A. and Mitra, D., Magnetic helicity transport in the advective gauge family. *Phys. Plasmas* 2011, **18**, 012903.
- Chan, K.-L., Rotating convection in f-boxes: faster rotation. *Astron. Nachr.* 2007, **328**, 1059–1062.
- Elperin, T., Kleorin, N. and Rogachevskii, I., Generation of large-scale vorticity in a homogeneous turbulence with a mean velocity shear. *Phys. Rev. E* 2003, **68**, 016311.
- Ghizaru, M., Charbonneau, P. and Smolarkiewicz, P.K., Magnetic cycles in global large-eddy simulations of solar convection. *Astrophys. J.* 2010, **715**, L133–L137.

- Gilman, P., Dynamically consistent nonlinear dynamos driven by convection in a rotating spherical shell. II – Dynamos with cycles and strong feedbacks. *Astrophys. J. Suppl.* 1983, **53**, 243–268.
- Glatzmaier, G.A., Numerical simulations of stellar convective dynamos. II – Field propagation in the convection zone. *Astrophys. J.* 1985, **291**, 300–307.
- Hubbard, A. and Brandenburg, A., Magnetic helicity flux in the presence of shear. *Astrophys. J.* 2011, **727**, 11.
- Hughes, D.W. and Proctor, M.R.E., Large-scale dynamo action driven by velocity shear and rotating convection. *Phys. Rev. Lett.* 2009, **102**, 044501.
- Jones, C.A. and Roberts, P.H., Convection-driven dynamos in a rotating plane layer. *J. Fluid Mech.* 2000, **404**, 311–343.
- Käpylä, P.J., On global solar dynamo simulations. *Astron. Nachr.* 2011, **332**, 43–50.
- Käpylä, P.J., Korpi, M.J. and Brandenburg, A., Large-scale dynamos in turbulent convection with shear. *Astron. Astrophys.* 2008, **491**, 353–362.
- Käpylä, P.J. and Brandenburg, A., Turbulent dynamos with shear and fractional helicity. *Astrophys. J.* 2009, **699**, 1059–1066.
- Käpylä, P.J., Mitra, D. and Brandenburg, A., Numerical study of large-scale vorticity generation in shear-flow turbulence. *Phys. Rev. E* 2009a, **79**, 016302.
- Käpylä, P.J., Korpi, M.J. and Brandenburg, A., Large-scale dynamos in rigidly rotating turbulent convection. *Astrophys. J.* 2009b, **697**, 1153–1163.
- Käpylä, P.J., Korpi, M.J. and Brandenburg, A., Alpha effect and turbulent diffusion from convection. *Astron. Astrophys.* 2009c, **500**, 633–646.
- Käpylä, P.J., Korpi, M.J. and Brandenburg, A., Open and closed boundaries in large-scale convective dynamos. *Astron. Astrophys.* 2010a, **518**, A22.
- Käpylä, P.J., Brandenburg, A., Korpi, M.J., Snellman, J.E. and Narayan, R., Angular momentum transport in convectively unstable shear flows. *Astrophys. J.* 2010b, **719**, 67–76.
- Käpylä, P.J., Korpi, M.J. and Brandenburg, A., The α effect in rotating convection with sinusoidal shear. *Mon. Not. R. Astron. Soc.* 2010c, **402**, 1458–1466.
- Käpylä, P.J., Korpi, M.J., Brandenburg, A., Mitra, D. and Tavakol, R., Convective dynamos in spherical wedge geometry. *Astron. Nachr.* 2010d, **331**, 73–81.
- Käpylä, P.J., Mantere, M.J. and Hackman, T., Starspots due to large-scale vortices in rotating turbulent convection. *Astrophys. J.* 2011, **742**, 34.
- Käpylä, P.J., Mantere, M.J. and Brandenburg, A., Cyclic magnetic activity due to turbulent convection in spherical wedge geometry. *Astrophys. J. Lett.* 2012, **755**, L22.
- Krause, F. and Rädler, K.H., *Mean-field Magnetohydrodynamics and Dynamo Theory*, 1980. (Oxford: Pergamon Press).
- Mantere, M.J., Käpylä, P.J. and Hackman, T., Dependence of the large-scale vortex instability on latitude, stratification and domain size. *Astron. Nachr.* 2011, **332**, 876–882.
- Miesch, M.S. and Toomre, J., Turbulence, magnetism, and shear in stellar interiors. *Ann. Rev. Fluid Mech.* 2009, **41**, 317–345.
- Mitra, D., Tavakol, R., Käpylä, P.J. and Brandenburg, A., Oscillatory migrating magnetic fields in helical turbulence in spherical domains. *Astrophys. J. Lett.* 2010, **719**, L1–L4.
- Moffatt, H.K., *Magnetic Field Generation in Electrically Conducting Fluids*, 1978. (Cambridge: Cambridge University Press).
- Nordlund, Å., Brandenburg, A., Jennings, R.L., Rieutord, M., Ruokolainen, J., Stein, R.F. and Tuominen, I., Dynamo action in stratified convection with overshoot. *Astrophys. J.* 1992, **392**, 647–652.
- Ossendrijver, M., The solar dynamo. *Astron. Astrophys. Rev.* 2003, **11**, 287–367.
- Parker, E.N., Hydromagnetic dynamo models. *Astrophys. J.* 1955, **121**, 491.
- Racine, É., Charbonneau, P., Ghizaru, M., Bouchat, A. and Smolarkiewicz, P.K., On the mode of dynamo action in a global large-eddy simulation of solar convection. *Astrophys. J.* 2011, **735**, 46.
- Rotvig, J. and Jones, C.A., Rotating convection-driven dynamos at low Ekman number. *Phys. Rev. E* 2002, **66**, 056308.
- Rüdiger, G., *Differential Rotation and Stellar Convection. Sun and Solar-type Stars*, 1989. (Berlin: Akademie Verlag).
- Rüdiger, G., Elstner, D. and Ossendrijver, M., Do spherical α^2 -dynamos oscillate? *Astron. Astrophys.* 2003, **406**, 15–21.
- Rüdiger, G. and Hollerbach, R., *The Magnetic Universe: Geophysical and Astrophysical Dynamo Theory*, 2004. (Weinheim: Wiley-VCH).
- Steenbeck, M., Krause, F. and Rädler, K.-H., Berechnung der mittleren Lorentz-Feldstärke für ein elektrisch leitendes Medium in turbulenter, durch Coriolis-Kräfte beeinflusster Bewegung. *Z. Naturforsch. A* 1966, **21**, 369–376.
- Steenbeck, M. and Krause, F., On the dynamo theory of stellar and planetary magnetic fields. I. AC dynamos of solar type. *Astron. Nachr.* 1969, **291**, 49–84.
- Stix, M., Differential rotation and the solar dynamo. *Astron. Astrophys.* 1976, **47**, 243–254.